

Photon-pair generation by intermodal spontaneous four-wave mixing in birefringent, weakly guiding optical fibers

K. Garay-Palmett,¹ D. Cruz-Delgado,² F. Dominguez-Serna,¹ E. Ortiz-Ricardo,² J. Monroy-Ruz,²
H. Cruz-Ramirez,² R. Ramirez-Alarcon,² and A. B. U'Ren²

¹*Departamento de Óptica, Centro de Investigación Científica y de Educación Superior de Ensenada,
Apartado Postal 360 Ensenada, BC 22860, México*

²*Instituto de Ciencias Nucleares, Universidad Nacional Autónoma de México, Apartado Postal 70-543, 04510 D.F., México*
(Received 6 July 2015; published 7 March 2016)

We present a theoretical and experimental study of the generation of photon pairs through the process of spontaneous four-wave mixing (SFWM) in a few-mode, birefringent fiber. Under these conditions, multiple SFWM processes are in fact possible, each associated with a different combination of transverse modes for the four waves involved. We show that in the weakly guiding regime, for which the propagation modes may be well approximated by linearly polarized modes, the departure from circular symmetry due to the fiber birefringence translates into conservation rules, which retain elements from azimuthal and rectangular symmetries: both OAM and parity must be conserved for a process to be viable. We have implemented a SFWM source based on a bowtie birefringent fiber, and have measured for a collection of pump wavelengths the SFWM spectra of each of the signal and idler photons in coincidence with its partner photon. We have used this information, together with knowledge of the transverse modes into which the signal and idler photons are emitted, as input for a genetic algorithm, which accomplishes two tasks: (i) the identification of the particular SFWM processes that are present in the source, and (ii) the characterization of the fiber used.

DOI: [10.1103/PhysRevA.93.033810](https://doi.org/10.1103/PhysRevA.93.033810)

I. INTRODUCTION

The process of spontaneous four-wave mixing (SFWM) [1] has, over the last decade and a half, become a viable alternative based on the $\chi^{(3)}$ nonlinearity of optical fibers for the generation of photon pairs, to the more established process of spontaneous parametric down-conversion (SPDC) in $\chi^{(2)}$ nonlinear crystals [2]. The implementation of SFWM sources with fibers, which support more than one transverse mode leads to a wealth of possibilities, some of which are explored in this paper.

The transverse modal content of a fiber can be exploited for increasing the transmission capacity in optical communication systems [3], and in nonlinear optics may be used for tuning the frequencies of operation [4,5]. In the context of $\chi^{(2)}$ nonlinear waveguide SPDC sources, the use of transverse modes has been explored in a number of papers [6–10]. Transverse spatial modes represent an essential feature of optical fibers; in this paper, we focus on the interplay of the spectral and transverse spatial mode degrees of freedom in the SFWM process. We show that the two-photon state obtained through SFWM in a fiber that supports more than one transverse mode in general exhibits hybrid entanglement in frequency and transverse mode [11]. Importantly, spatial entanglement based on transverse fiber modes is scalable to higher dimensions as controlled by the number of supported fiber modes, unlike polarization entanglement, which is limited to a dimension of 2. A highly important feature of higher-order fiber modes is that they may carry orbital angular momentum (OAM), so that transverse mode entanglement can imply the presence of OAM entanglement.

Building on previous work from our group [12], we have concentrated on the use of few-mode, weakly guiding,

birefringent fibers [13–16] as a useful experimental platform for the study of two-photon states, which can exhibit hybrid entanglement in frequency and transverse mode. In such fibers, while all six electromagnetic field components of the supported modes are nonzero, they may be well approximated by linearly polarized (LP) modes. If multiple transverse modes are supported, a number of SFWM processes are possible each involving a distinct combination of transverse modes for the four participating waves: pump 1, pump 2, signal, and idler. We discuss how in the absence of full circular symmetry the supported modes may be well described by linearly polarized (LP) modes with well-defined even or odd parities. It is known that while OAM conservation is expected for circularly symmetric guided-wave SPDC and SFWM sources, this conservation rule becomes parity conservation for sources with rectangular symmetry. We show that SFWM in birefringent fibers retain elements from both azimuthal and Cartesian symmetries: i.e., both OAM and parity are conserved. For a fiber that supports M modes, there may be up to M^4 intermodal SFWM processes; we describe how parity and OAM conservation rules define which of these M^4 processes can actually take place.

We present experimental data of SFWM spectra obtained for a birefringent bowtie fiber, for a number of different pump wavelengths. This data shows evidence of three separate SFWM processes, manifested by three pairs of energy-conserving peaks. An analysis of the processes that conserve both OAM and parity, together with a genetic algorithm, which takes the measured spectra along with the known propagation modes corresponding to each of the six peaks as input, enables us to identify the specific SFWM processes present in our source, and also yields a characterization of the fiber used.

II. INTERMODAL SPONTANEOUS FOUR-WAVE MIXING IN BIREFRINGENT FIBERS

A. Two-photon state for multiple intermodal SFWM processes

In an optical fiber that supports more than one transverse mode, several intermodal SFWM processes can take place. The resulting two-photon state is then a coherent superposition of the contributions from the different processes, each of which is associated with a particular combination of transverse modes for the four waves involved (pump 1, pump 2, signal, and idler) [12]. Here we will consider experimental situations where while the two pumps may be nondegenerate in transverse mode, they are spectrally degenerate.

As will be discussed in detail below, among all possible combinations of supported modes for the four waves, those that (i) are phase matched, and (ii) have a nonzero transverse mode overlap, lead to allowed SFWM processes. If there are N such allowed processes (in the spectral range of interest), the two photon state in general exhibits hybrid entanglement in frequency and in transverse mode, and is given by $|\Psi\rangle = |\text{vac}\rangle + \eta|\Psi_2\rangle$, with

$$|\Psi_2\rangle = \sum_{j=1}^N \sqrt{W_{j1}W_{j2}} \mathcal{O}_j(\alpha_j, \beta_j, \mu_j, \nu_j) \times \int d\omega_s \int d\omega_i f_j(\omega_s, \omega_i) \hat{a}^\dagger(\omega_s; \mu_j) \hat{a}^\dagger(\omega_i; \nu_j) |\text{vac}\rangle, \quad (1)$$

where for process j , $\hat{a}^\dagger(\omega_s; \mu_j)$ [$\hat{a}^\dagger(\omega_i; \nu_j)$] is the creation operator for the signal (idler) mode with frequency ω_s (ω_i) propagating in transverse spatial mode μ_j (ν_j), and where the pump 1 (pump 2) wave propagates in transverse mode α_j (β_j) with power W_{j1} (W_{j2}). $\mathcal{O}_j(\alpha_j, \beta_j, \mu_j, \nu_j)$ is the transverse mode overlap between the four waves, expressed in terms of the transverse electric field distribution $g(\xi; \rho^\perp)$, for transverse mode ξ and dependent on the the transverse position ρ^\perp , as

$$\mathcal{O}_j(\alpha_j, \beta_j, \mu_j, \nu_j) = M_j \int d^2\rho^\perp g(\alpha_j; \rho^\perp) g(\beta_j; \rho^\perp) \times g^*(\mu_j; \rho^\perp) g^*(\nu_j; \rho^\perp). \quad (2)$$

Note that in writing Eq. (2), we have assumed that the dependence on frequency for each of the transverse electric field distributions $g(\xi; \rho^\perp)$ may be neglected. Also, M_j is a normalization constant chosen so that the sum over all j of $|\mathcal{O}_j(\alpha_j, \beta_j, \mu_j, \nu_j)|^2$ yields unity.

For process j , $f_j(\omega_s, \omega_i)$ represents the joint spectral amplitude (JSA), which is determined by the phase-matching characteristics and is given by [17]

$$f_j(\omega_s, \omega_i) = \int d\omega A(\omega) A(\omega_s + \omega_i - \omega) \text{sinc}\left[\frac{L}{2} \Delta k_j\right], \quad (3)$$

written in terms of the fiber length L and the (degenerate) pump spectral envelope $A(\omega)$; the function $I_j(\omega_s, \omega_i) = |f_j(\omega_s, \omega_i)|^2$ is referred to as the joint spectral intensity (JSI). In Eq. (3), Δk_j represents the phase mismatch given by

$$\Delta k_j = k(\omega; \alpha_j) + k(\omega_s + \omega_i - \omega; \beta_j) - k(\omega_s; \mu_j) - k(\omega_i; \nu_j) - \phi_{NLj} \quad (4)$$

given in terms of the wave number $k(\omega; \xi)$ for transverse mode ξ and frequency ω ; ϕ_{NLj} is a nonlinear contribution determined by self- and cross-phase modulation [17].

Note that while a number of works have studied in detail the longitudinal phase-matching properties, as defined by the JSA function [see Eq. (3)], in the theoretical part of this paper we focus on the transverse mode overlap term $\mathcal{O}_j(\alpha_j, \beta_j, \mu_j, \nu_j)$ and on the new physics, which may be derived henceforth.

While the theory presented so far is general and can be applied to any type of fiber, we are interested in particular in SFWM sources implemented with birefringent fibers. Knowledge of the modes which are supported by the SFWM fiber is required for a theoretical description of the two-photon state. Our work, presented below, is based on a fiber in which the circular symmetry of the fiber is (slightly) broken by the birefringence introduced by two stress rods on either side of the core. In Sec. II B, below, we discuss how the fiber modes are well described by linearly polarized (LP) modes, appropriately modified by polarization and parity.

Let us note that if a single SFWM process [corresponding to a particular value of j in Eq. (1)] were to be postselected, then the resulting two-photon state can be entangled in frequency but is otherwise unentangled; in particular, since the postselected signal and idler photons propagate in known transverse modes μ_j and ν_j , spatial and mixed spatial-spectral entanglement is suppressed. Each process has an efficiency defined by the overlap between the four waves involved $\mathcal{O}_j(\alpha_j, \beta_j, \mu_j, \nu_j)$. For M supported modes, we can have in principle up to M^4 SFWM processes, so that an important question, which we address in this paper is which of these M^4 processes actually take place in a given situation. We will show for the particular case of linearly polarized (LP) modes, that this mode overlap is nonzero if both OAM and parity are conserved. This is crucial for an understanding of the two-photon source, because it enables the identification of the processes that are viable. It is important to point out that the number of viable processes can be drastically reduced by OAM and parity conservation from the M^4 possible processes.

We point out that phase-matching properties are such that typically signal and idler emission frequencies are correlated to the particular spatial modes involved in each process. This implies that the postselection referred to in the previous paragraph can be accomplished in a straightforward manner through spectral filtering. If, however, no postselection is carried out then the two-photon state is given by a coherent sum as indicated in Eq. (1). In this case, the two-photon state can exhibit hybrid frequency-transverse mode entanglement. While OAM and parity for the overall two-photon state are not well defined, and therefore it is unclear how to formulate OAM and parity conservation rules for this overall state, these quantities must be conserved, as we show in Sec. II C below, on a process-by-process basis.

In this paper, we concentrate on cross-polarized SFWM sources implemented with few-mode, weakly guiding, birefringent fibers. The essential advantage of such SFWM sources is that the fiber birefringence results in a shift (with respect to a copolarized SFWM process in nonbirefringent fiber) in the phase-matching condition leading to signal and idler frequencies ω_s and ω_i , which are sufficiently removed from the pump frequency ω_p to avoid Raman contamination, while

group velocity matching conditions can be fulfilled permitting various types of engineered spectral correlations [18]. Such fibers have indeed been used as the basis for a number of recent experiments [13–16]. In this paper we aim to provide a complete theoretical framework, which permits the full description of the SFWM two-photon state produced in such fibers. This framework must include reliable knowledge of the transverse modes involved, incorporating the effect of parity and birefringence, as will be discussed in Sec. II B. An important aspect, discussed in Sec. II C, is how parity and OAM conservation can help define which SFWM processes actually take place. The dispersion model that we have used, including polarization and parity birefringence, required for carrying our specific simulations of the two-photon state, is described in Sec. II D.

B. Transverse modes in weakly guiding, birefringent fibers

A conventional optical fiber exhibits a step refractive index profile. It comprises a core with radius r_0 and refractive index n_1 , and a cladding with refractive index n_2 ($n_1 > n_2$); the electromagnetic formalism for such fibers is well known [19]. While the exact propagating modes are hybrid in the sense that all six components of the electromagnetic field are nonzero, for fibers characterized by a low dielectric contrast ($n_1 - n_2 \ll 1$), it is well known that the propagating modes are approximately linearly polarized. Thus, for circularly symmetric fibers with a low dielectric contrast, transverse modes are well described by the LP_{lm} family of modes, where $l = 0, 1, 2, \dots$ and $m = 1, 2, \dots$ indicate the number of maxima of the spatial profile along the azimuthal and radial directions, respectively. Note that the mode index l is related to the orbital angular momentum (OAM) of light; in particular, a mode with subindex l corresponds to a linear combination of contributions with azimuthal dependence $\exp(\pm il\phi)$, i.e., with topological charge $\pm l$. It can be shown that an LP_{lm} mode arises from the superposition of the nearly degenerate exact modes $HE_{l+1,m}$ and $EH_{l-1,m}$; while neither of these modes is linearly polarized, the sum is in fact nearly linearly polarized [19].

In our work we are interested in birefringent fibers that depart from being circularly symmetric. Let us note that for circularly symmetric fibers, we are free to express the azimuthal dependence of the LP modes in an exponential $\{\exp(il\phi), \exp(-il\phi)\}$ or in a $\{\sin(l\phi), \cos(l\phi)\}$ basis. However, in the presence of fiber birefringence for which azimuthal symmetry is broken, modes have a well-defined even or odd parity and modes with an exponential $\exp(\pm il\phi)$ azimuthal dependence are in fact not supported. Thus, for a birefringent fiber the propagation modes are correctly expressed in the sine or cosine basis, with an appropriate parity-dependent propagation constant. This is consistent with the fact that the SFWM photons emitted by our source, see Sec. III below, indeed have well-defined parities.

Each propagation mode has two additional properties, besides the number of radial and azimuthal maxima, which are essential in our analysis: polarization and parity. In fact, the fundamental mode LP_{01} actually represents two modes, the x -polarized LP_{01}^x and the y -polarized LP_{01}^y modes, which become degenerate (i.e., have the same propagation constant) in the case of circularly symmetric fibers. For higher-order

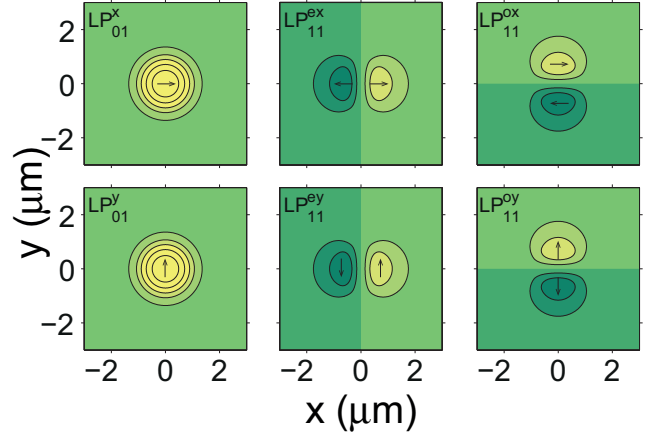


FIG. 1. Unfolding of the LP_{01} and LP_{11} modes.

modes, parity becomes important [19,20], so that for example the mode LP_{11} actually represents the four modes LP_{11}^{ex} , LP_{11}^{ey} , LP_{11}^{ox} , and LP_{11}^{oy} , where e (o) signifies even (odd) parity. Again, while these four modes are degenerate for circularly symmetric fibers, in the case of a birefringent fiber they become nondegenerate and must be taken into account separately. A graphical summary of this unfolding of the LP_{01} and LP_{11} modes into six separate modes is shown in Fig. 1. Note that all modes LP_{lm} with $l \geq 1$ likewise unfold into four separate modes, which become nondegenerate in fibers that depart from circular symmetry.

The transverse mode set for birefringent fibers is consequently well represented by the linearly polarized (LP) modes, with four labels, written as LP_{lm}^{pq} . While $l = 0, 1, 2, \dots$ and $m = 1, 2, \dots$ indicate the number of maxima of the spatial profile along the azimuthal and radial directions, respectively, $p = x(y)$ indicates that the mode is polarized along the x (y) direction and $q = e(o)$ indicates the mode has even (odd) parity. Note that the x (y) polarization in our case is defined as parallel to the slow axis (fast axis) of the birefringent fiber used. Note, also, that while the parity can be even or odd for all values $l \geq 1$, $l = 0$ modes always have even parity. The subscripts $\alpha_j, \beta_j, \mu_j, \nu_j$ in Eqs. (2) and (4) then represent particular combinations of values for the four mode indices l and m , p , and q .

The transverse electric field distribution for mode LP_{lm}^{pq} , expressed in polar coordinates r and ϕ , can be factored into radial and azimuthal factors as follows

$$g_{lm}^{pq}(r, \phi) = F_{lm}^{pq}(r)G_l^q(\phi). \quad (5)$$

In Eq. (5), the radial factor is given in terms of the l th-order Bessel function of the first kind $J_l(\cdot)$ and the l th-order modified Bessel function of the second kind $K_l(\cdot)$, as

$$F_{lm}^{pq}(r) = \begin{cases} J_l(u_{lm}^{pq}r), & r < r_0 \\ K_l(v_{lm}^{pq}r), & r > r_0 \end{cases}, \quad (6)$$

where r_0 is the core radius and where

$$u_{lm}^{pq} = \sqrt{k_1^2 - (k_{lm}^{pq})^2} \quad v_{lm}^{pq} = \sqrt{(k_{lm}^{pq})^2 - k_2^2} \quad (7)$$

are parameters defined in terms of the wave numbers for frequency ω of the propagation mode, k_{lm}^{pq} , as well as wave

numbers corresponding to the core, k_1 , and the cladding, k_2 , expressed as

$$k_{lm}^{pq} = n_{lm}^{pq} \omega / c \quad k_1 = n_1 \omega / c \quad k_2 = n_2 \omega / c. \quad (8)$$

In the equation above, n_{lm}^{pq} represents the effective index in the fiber of the propagation mode. Note that for the specific case $l = 0$, there is no azimuthal dependence and $G_0^q(\phi) = 1$ if $q = 1$ (even parity), while $G_0^q(\phi)$ is undefined if $q = -1$ (odd parity), i.e., the modes with $l = 0$ necessarily have an even parity. For $l \geq 1$,

$$G_l^q(\phi) = \begin{cases} \cos(l\phi), & q = 1 \quad (\text{even mode}) \\ \sin(l\phi), & q = -1 \quad (\text{odd mode}) \end{cases}. \quad (9)$$

We will now proceed to investigate the form which the mode overlap [see Eq. (2)] takes for LP modes.

C. Conservation of orbital angular momentum and parity in SFWM

The question of whether OAM and parity are conserved for the spontaneous parametric down-conversion (SPDC) process has been addressed by a number of authors. OAM conservation was assumed to hold in the early work on OAM entanglement with nonguided SPDC [21]; it was identified then that OAM conservation leads naturally to OAM entanglement. It was later determined that in fact OAM conservation is only to be expected in those particular cases for which the interaction Hamiltonian is azimuthally symmetric [22–25]. Thus, in a number of nonguided source configurations including bulk-crystal type-II, as well as type-I source designs for which Poynting vector walk off cannot be ignored (e.g., derived from strong pump focusing or a long crystal), OAM is not conserved. In the case of guided SPDC, i.e., occurring in a nonlinear $\chi^{(2)}$ waveguide, source symmetries dictate the conservation rules [26]. While azimuthally symmetric circular waveguides lead to an OAM conservation rule, rectangular waveguides lead to a parity, rather than OAM, conservation rule [10,27]. Our own SFWM source is characterized by a cylindrical fiber core with a (slight) deviation from azimuthal symmetry which translates into nonazimuthally symmetric $l \geq 1$ modes. It is very interesting that for this source, elements are retained from both circular and Cartesian symmetries: as we show in this section, both OAM and parity are conserved on a process-by-process basis.

Let us note that classical, i.e., stimulated, three- and four-wave mixing processes are a close relative of the spontaneous four-wave mixing process studied in this paper so that our discussion, including the physics of parity and OAM conservation, of course, is related to the similar effects observed classically [28]. In particular, recent work has addressed these issues for stimulated four-wave mixing [29,30]. The quantum-mechanical treatment presented here is aimed at enabling the design of a new generation of fiber-based photon pair sources with hybrid entanglement in frequency and in transverse mode.

In a fiber that supports multiple transverse modes, each possible combination of transverse modes amongst the four participating waves can result in a SFWM process provided that two conditions are fulfilled: (i) the four waves are appropriately phase matched at given pump and generation frequencies,

i.e., $\Delta k_j = 0$ [see Eq. (4)], or at least approximately phase matched as $|L\Delta k_j| \leq 2\pi$, and (ii) these four waves have a nonvanishing overlap. In a situation where there are M transverse modes available for each wave, there are M^4 possible processes. For example, if the LP₀₁ and LP₁₁ are supported (which become six nondegenerate modes in the case of a birefringent fiber), there are then $6^4 = 1296$ possible processes. We show below that the second condition, i.e., a nonvanishing mode overlap, translates for the specific case of linearly polarized modes into conservation rules, which may be used to greatly reduce the number of viable processes.

Let us consider the case where each wave is described by LP modes, so that for process j the pump-1 (pump-2) wave α_j (β_j) becomes characterized by four indices: l_{j1} , m_{j1} , p_{j1} , and q_{j1} (l_{j2} , m_{j2} , p_{j2} , and q_{j2}). Likewise, the signal (idler) wave μ_j (ν_j) becomes characterized by four indices l_{js} , m_{js} , p_{js} , and q_{js} (l_{ji} , m_{ji} , p_{ji} , and q_{ji}). The fact that for LP modes the transverse electric field distribution $g_{lm}^{pq}(r, \phi)$ is factorable into radial and azimuthal contributions, implies that the mode overlap $\mathcal{O}_j(\alpha_j, \beta_j, \mu_j, \nu_j)$ may be likewise factored into radial and azimuthal contributions, as

$$\mathcal{O}_j(\alpha_j, \beta_j, \mu_j, \nu_j) = \mathcal{O}_j^r \mathcal{O}_j^\phi, \quad (10)$$

in terms of radial and azimuthal overlap integrals, \mathcal{O}_j^r and \mathcal{O}_j^ϕ , as follows

$$\begin{aligned} \mathcal{O}_j^r &= \int_0^\infty r dr F_{l_{j1}m_{j1}}^{p_{j1}q_{j1}}(r) F_{l_{j2}m_{j2}}^{p_{j2}q_{j2}}(r) [F_{l_{js}m_{js}}^{p_{js}q_{js}}(r)]^* [F_{l_{ji}m_{ji}}^{p_{ji}q_{ji}}(r)]^* \\ \mathcal{O}_j^\phi &= \int_0^{2\pi} d\phi G_{l_{j1}}^{q_{j1}}(\phi) G_{l_{j2}}^{q_{j2}}(\phi) [G_{l_{js}}^{q_{js}}(\phi)]^* [G_{l_{ji}}^{q_{ji}}(\phi)]^*. \end{aligned} \quad (11)$$

For the analysis below, we will focus on the azimuthal overlap \mathcal{O}_j^ϕ , which may be expressed as

$$\mathcal{O}_j^\phi = \delta_{\Delta q_j} (\delta_{\Delta l_j^{+++}} + \delta_{\Delta l_j^{++}} + \dots + \delta_{\Delta l_j^{---}}), \quad (12)$$

where the quantity within the brackets contains terms defined by all eight possible combinations of signs for l_{j2} , l_{js} , and l_{ji} . In Eq. (12), δ_n , with integer n , represents a one-argument Kronecker δ (which vanishes unless $n = 0$, in which case the δ yields unity). Note that in writing Eq. (12) we have defined a parity nonconservation parameter for process j , Δq_j , as follows

$$\Delta q_j = q_{j1}q_{j2} - q_{js}q_{ji}, \quad (13)$$

as well as a family of OAM nonconservation parameters for process j

$$\begin{aligned} \Delta l_j^{+++} &= l_{j1} + l_{j2} + l_{js} + l_{ji} \\ \Delta l_j^{-++} &= l_{j1} - l_{j2} + l_{js} + l_{ji} \\ \dots & \\ \Delta l_j^{---} &= l_{j1} - l_{j2} - l_{js} - l_{ji}, \end{aligned} \quad (14)$$

for all eight combinations of signs for l_{j2} , l_{js} , and l_{ji} .

It is clear from Eq. (12) that in order for the azimuthal overlap to be nonzero for a given process j , the following two conditions must be observed: (i) $\Delta q_j = 0$ and (ii) at least one

of the eight terms within the brackets, each corresponding to a different combination of signs in front of the topological charges for three of the waves, must be nonzero, leading to the condition that at least one Δl_j parameter must vanish.

The first of the above conditions tells us that the mode overlap vanishes unless $q_{j_1}q_{j_2} = q_{j_3}q_{j_4}$, i.e., the parity of the pump waves must match the parity of the generated SFWM photons, which is a statement of parity conservation.

In order to interpret physically the second condition, let us consider the LP_{lm}^{pq} modes, expressed in the sine or cosine basis, which is consistent with the loss of circular symmetry in our birefringent fiber, see Eqs. (5) and (9). Note that while these modes do not contain a phase singularity and therefore do not carry OAM, they are in fact, for $l \geq 1$, the coherent addition of two subadjacent optical vortices with topological charges l and $-l$. The second of the above conditions is then fulfilled if the sum of the topological charge values for all four waves, with any combination of signs in front of each one, is zero. In other words, this second condition is fulfilled if OAM is conserved, i.e., the sum of the topological charges for the two pumps matches the sum of the topological charges for the two generated photons, when any of the two subadjacent vortices is selected for each of these four waves.

It is important to point out that the parity and OAM conservation rules presented here cannot apply to the overall two-photon state; indeed, it is not clear how to define parity and OAM for the overall two-photon state. Thus, parity and OAM conservation rules apply on a process-by-process basis, and determine whether a particular SFWM process j is viable.

D. Simplified model for dispersion properties of birefringent fibers

Birefringent fibers allow cross-polarized phase matching in SFWM [12–15,31]. In this paper, we focus on processes of the kind $xx-yy$, in which the pump and the emitted photons have orthogonal polarizations. While fiber birefringence is essential in our experimental implementation so as to ensure phase matching, it is in fact important in other ways. Indeed, such a cross-polarized scheme simplifies the separation of SFWM from pump photons at the fiber output, and contributes to minimize the noise background produced by spontaneous Raman scattering [32]. For an optimal implementation of this configuration it is desirable that the state of polarization of the waves involved remain unchanged along the fiber, which becomes viable in highly birefringent fibers, known as polarization maintaining fibers, for which the difference in propagation constant for the two orthogonal polarizations is obtained by designing elliptical cores or including panda- or bowtie-type stress rods into the cross section [33].

The degeneracy of modes with different polarization and parity is lifted in this kind of fibers due to the lack of azimuthal symmetry. Thus, modes LP_{lm}^{ex} , LP_{lm}^{ey} , LP_{lm}^{ox} , and LP_{lm}^{oy} all have a different propagation constant [34].

In order to specify the effective refractive index of propagating modes in highly birefringent fibers, we use a simple model based on the treatment for circularly symmetric step index fibers in the weakly guiding approximation [19]. Assuming that n_0 is the effective refractive index for a specific LP_{lm} mode (with $l \geq 1$) in the circularly symmetric fiber, we model

the refractive indices of the four unfolded modes as follows

$$\begin{aligned} n_{ey} &= n_0, & n_{oy} &= n_0 + \Delta_p, \\ n_{ex} &= n_0 + \Delta, & n_{ox} &= n_0 + \Delta + \Delta_p, \end{aligned} \quad (15)$$

where Δ and Δ_p are the polarization and parity birefringences, respectively. Note that for $l = 0$ modes, odd parity is undefined, so that these relations simplify to

$$n_y = n_0 \quad n_x = n_0 + \Delta. \quad (16)$$

From these definitions the propagation constant for each mode can then be calculated, which allows us to explore the phase-matching properties for all potential SFWM processes.

III. EXPERIMENTAL IMPLEMENTATION

The SFWM source used in our experiments, sketched in Fig. 2, is similar to the one used in our papers [12,18]. We employ as pump for the SFWM process a picosecond mode-locked Ti:sapphire laser (76MHz repetition rate and ~ 0.5 nm bandwidth with a central wavelength which in our experiment is tuned from 690–720 nm). The pump beam, filtered with a prism-based spectral bandpass filter (PF) with ~ 50 mW power, is coupled into a 14.5 cm length of bowtie birefringent fiber using an aspheric lens with 8 mm focal length (L1); the polarization in the fiber is set parallel to the fiber's slow axis using a half wave plate (HWP1). We generate photon pairs in this fiber through cross-polarized SFWM so that the signal and idler photons are polarized parallel to the fiber's fast axis (see inset of Fig. 2). The photon pairs are outcoupled from the fiber

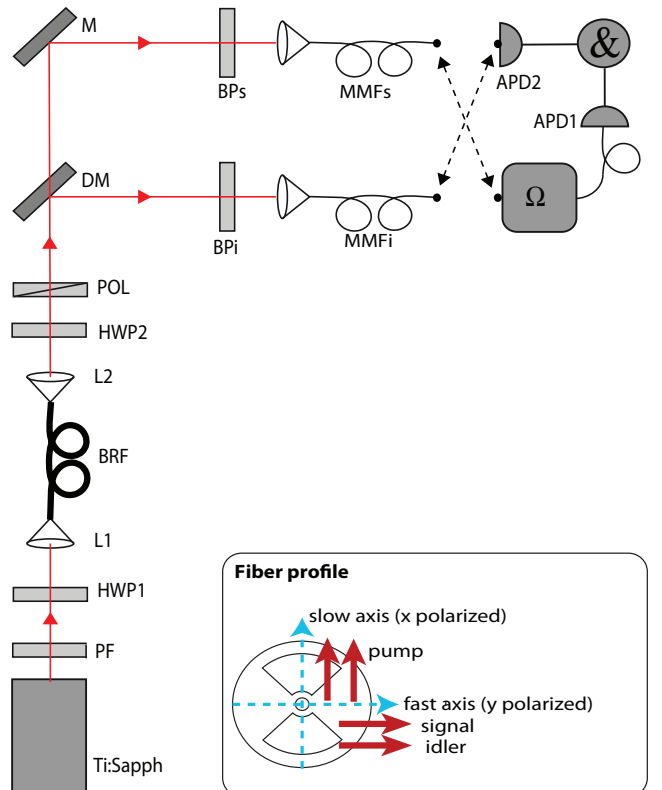


FIG. 2. Experimental setup.

using a second aspheric lens with 8 mm focal length (L2) and their polarization is set to horizontal using a second half wave plate (HWP2); a Glan-Thompson polarizer (POL) reduces the remaining pump power by a factor equal to the extinction ratio of $\sim 10^5$. The photon pairs are frequency nondegenerate, emitted in spectral bands placed symmetrically around the pump; they are split using a dichroic mirror (DM) followed by bandpass filters (BPs and BPi) centered at the signal and idler photons for further pump suppression.

Our primary aim is to measure the signal and idler emission spectra, as a function of the pump wavelength. For this purpose, we rely on spectrally resolved, coincidence photon counting. For a given pump central frequency, which we scan from 690–720 nm, we couple the idler ($\lambda < \lambda_p$) and signal ($\lambda > \lambda_p$) photons into separate multimode fibers, MMFi and MMFs. For spectrally resolved detection, we employ a scanning grating-based monochromator (Ω), which has been fitted with

multimode fiber input and output ports. While MMFi serves as input for Ω , with the output of Ω directed to a silicon avalanche photodiode (APD1), fiber MMFs leads directly to a second avalanche photodiode (APD2). We then monitor the coincidence rate at APD1 and APD2, with accidental counts subtracted, as a function of the central transmission frequency of Ω . In this manner we are able to measure the signal-photon spectrum in coincidence with the corresponding (spectrally unresolved) idler photon. Subsequently, we reverse the role of the two photons so as to measure the idler-photon spectrum in coincidence with the (spectrally unresolved) signal photon.

In Fig. 3 we show our experimental results. In Fig. 3(a) we show a collection of idler-photon ($\lambda < \lambda_p$) spectra for a number of different pump wavelengths within the range 690–720 nm. In Fig. 3(b) we show the corresponding signal-photon ($\lambda > \lambda_p$) spectra. It is apparent from these plots, especially for the lower pump wavelengths, that the SFWM

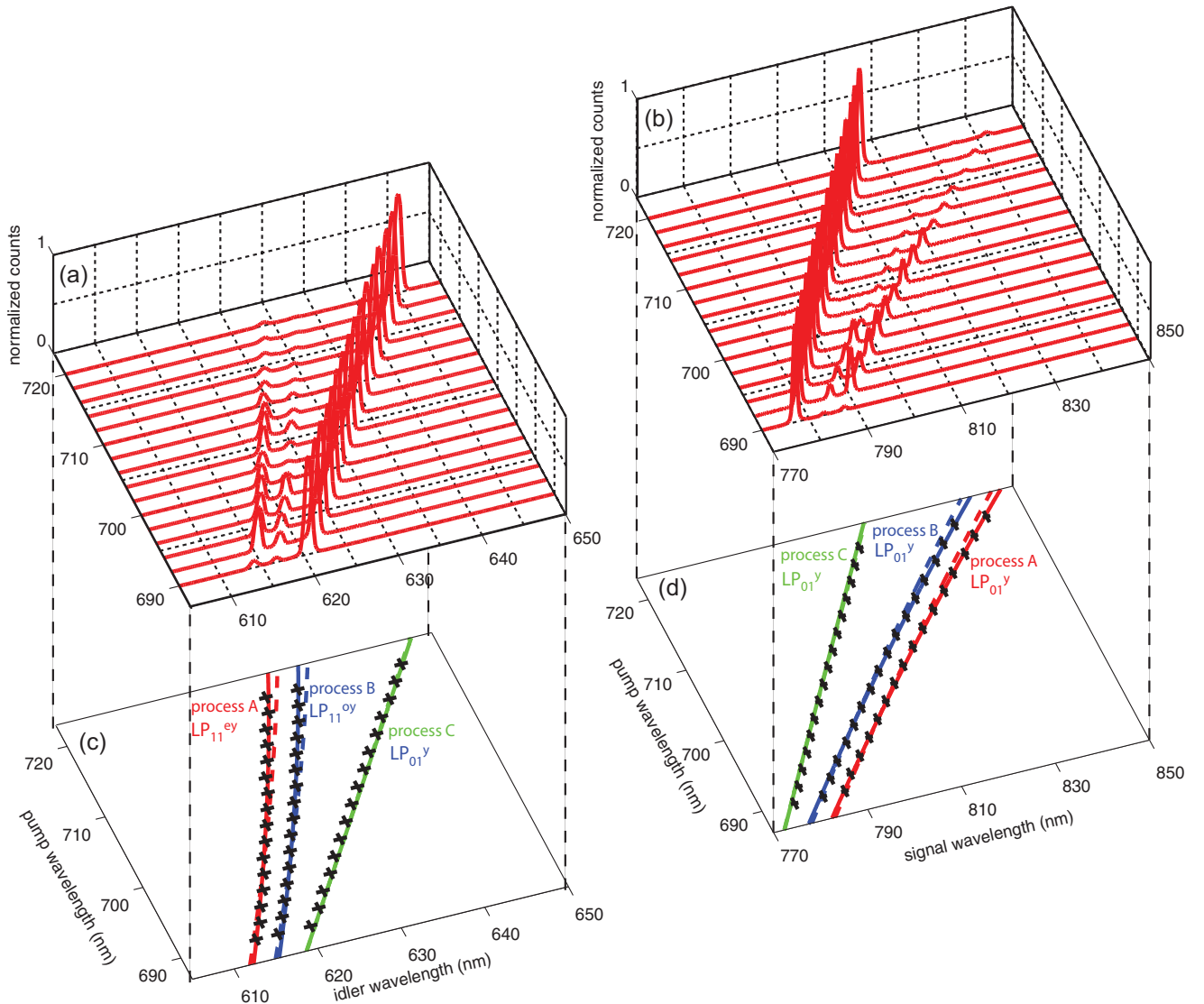


FIG. 3. (a) and (b): Measured SFWM spectra composed of three pairs of signal-idler energy-conserving peaks, for a number of pump wavelengths within the range 690–720 nm, (c) and (d): SFWM wavelengths as a function of the pump wavelength for each of the three inferred processes; horizontal bars represent the signal or idler emission bandwidth while vertical bars indicate the pump bandwidth.

spectra are in the form of three pairs of energy-conserving peaks. One of the pairs of peaks (the one which involves signal and idler wavelengths closest to the pump wavelength) leads to a higher count rate (by about one order of magnitude, as compared to the other two pairs of peaks. The three pairs of peaks are present for all of the pump wavelengths considered, although for the larger pump wavelengths two of them are much reduced in count rate; this is in all likelihood because the pump approaches the cutoff wavelengths for the LP_{11}^{ex} and LP_{11}^{ox} modes, which serve as pumps for processes *A* and *B* [35]. In Fig. 3(c) we show the location of each of the three idler-photon peaks, directly obtained from the peak maxima in Fig. 3(a); for each of the experimental points, the horizontal bar indicates the width of the corresponding SFWM peak, while the vertical bar represents the pump bandwidth. Figure 3(d) shows the corresponding signal-photon emission wavelengths as a function of the pump wavelength, obtained from Fig. 3(b).

It is to be expected that each of the pairs of peaks discussed in the previous paragraph is associated with a separate SFWM process, defined by a particular combination of transverse modes for the four waves involved. In order to explore this, it is helpful to measure the transverse mode into which the signal and idler photons are emitted for each pair of peaks. As reported in Ref. [18], we have employed a combination of spectrally and spatially resolved photon counting in order to measure the transverse spatial distribution associated with each of the six peaks in Fig. 3; we have indicated in Figs. 3(c) and 3(d) the measured transverse mode next to each of the six curves. Note that these transverse modes remain unchanged for the whole range of pump wavelengths considered.

IV. ANALYSIS OF EXPERIMENTAL RESULTS

Our measurements of frequency-resolved coincidence rates suggest (for all pump frequencies considered within the range 690–720 nm) the presence of three separate SFWM processes, where each process contributes one pair of energy-conserving peaks. Qualitatively, all pump wavelengths lead to the same behavior, except that the signal and idler wavelengths shift towards the IR as the pump wavelength is increased (see Fig. 3). An analysis of the phase-matching properties in the fiber is needed in order to correctly identify the SFWM process, which gives rise to each measured pair of spectral peaks. Such an analysis demands knowledge of the chromatic dispersion and of the modes supported by the fiber. With the information provided by the manufacturer and based on measurements of the spatial profile of the generated photons reported in Ref. [18], we were able to identify that our bowtie fiber supports two propagation modes within the spectral range relevant in the experiment: LP_{01} and LP_{11} . Nevertheless, as was explained in Sec. II B, these two modes in fact unfold, in a birefringent fiber, into six nondegenerate modes, which leads to $6^4 = 1296$ possible SFWM processes. Restricting our attention to cross-polarized processes of the type xx - yy , as is done in our experiment, leaves $3^2 \times 3^2 = 81$ processes. Additionally, by invoking the conservation of OAM and parity (see Sec. II C) it can be shown that only 15 processes are actually viable. Thus, each of the three pairs of spectral peaks observed in the experiment could result from one of these

TABLE I. List of the 15 cross-polarized xx - yy SFWM processes, which conserve both OAM and parity.

	p1	p2	$s(\lambda > \lambda_p)$	$i(\lambda < \lambda_p)$
peaks A	01x	11ex	01y	11ey
peaks B	01x	11ox	01y	11oy
peaks C	01x	01x	01y	01y
	11ex	11ex	01y	01y
	11ox	11ox	01y	01y
others	01x	01x	11ey	11ey
	01x	01x	11oy	11oy
	01x	11ex	11ey	01y
	01x	11ox	11oy	01y
	11ex	11ex	11ey	11ey
	11ex	11ex	11oy	11oy
	11ex	11ox	11ey	11oy
	11ex	11ox	11oy	11ey
	11ox	11ox	11ey	11ey
11ox	11ox	11oy	11oy	

15 processes, subject to the phase-matching constraint [see Eq. (4)].

Note that while the transverse modes in which each of the SFWM photons is generated, within each of the three peaks, is known from our experimental measurements (as reported in Ref. [18]), the transverse modes in which the pump waves propagate cannot easily be determined from the experiment. Table I lists all 15 processes identified in the previous paragraph, classified into four mutually exclusive groups, where we have taken into account the measured transverse modes for the SFWM photons: (i) a single process that is compatible with pair of peaks *A*; (ii) a single process that is compatible with pair of peaks *B*; (iii) three processes that are compatible with pair of peaks *C*; and (iv) those processes that are not compatible with any of the three pairs of peaks.

Note that the description used in this paper, including the unfolding of LP modes according to parity and polarization, is an improvement over the model used in our earlier paper [12]. Note also that a reliable theoretical description of the fiber used in Ref. [12] is complicated on account of its very thin inner cladding (the space between the stress-applying rods and the core): different transverse modes extend to varying degrees outwards from the core, and some may reach the stress-applying rods. This implies that a simple dispersion model based on the step index fiber with corrections due to birefringence parameters is no longer sufficient. In this work we have used a fiber with the stress rods sufficiently removed from the core so that the evanescent tails of the transverse modes are fully contained by the inner cladding.

We have implemented a numerical strategy which accomplishes two tasks: it identifies (i) the processes (from the groups in Table I), which optimize the simultaneous phase matching for all three pairs of peaks, and (ii) the fiber parameters $\{r_0, NA, \Delta, \Delta_p\}$. For the particular case in question the first task is trivial for two of the three pairs of peaks since there is a single process available. The search in the parameter space $\{r_0, NA, \Delta, \Delta_p\}$ is executed exploiting a genetic algorithm (GA). In our GA, each individual is formed by the values of the

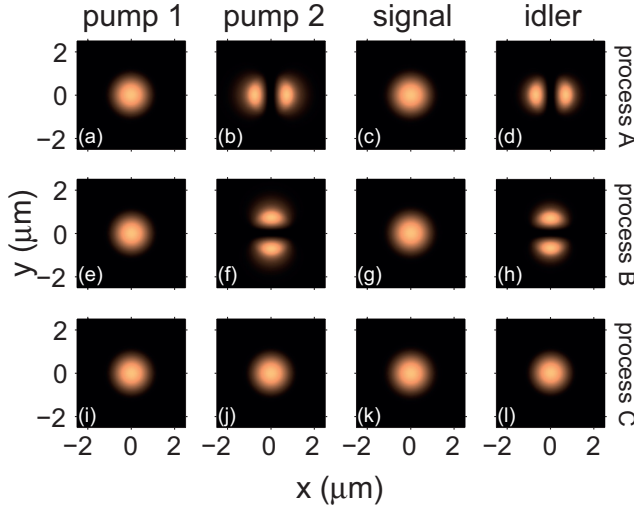


FIG. 4. Transverse modes participating in each of processes *A* (first row), *B* (second row), and *C* (third row). The columns correspond to the four waves involved in the SFWM process: pump 1, pump 2, signal, and idler.

four fiber parameters, and a fitness function (FF) is defined as $\Delta k_T = |\Delta k_A + \Delta k_B + \Delta k_C|$ (with $\Delta k_A/\Delta k_B/\Delta k_C$ the phase mismatch for process *A/B/C*, evaluated at the frequencies associated with each of the three pairs of peaks), with greater fitness associated with lower values of Δk_T . A population of individuals evolve through successive generations of children created from the forebears by three mechanisms: (i) the fittest ones (elite) are reproduced intact, (ii) combination of parents, or crossover, and (iii) the introduction of random mutations. Note that in each generation step of the GA, all possible SFWM processes for each pair of peaks are tested retaining the combinations of processes, which minimize the FF.

It is worth noting the FF can be defined for the three pairs of peaks obtained for a particular choice of pump wavelength or for collective data derived from m_p pump wavelengths; in the latter case, the definition of Δk_T is adjusted so that $3 \times m_p \Delta k_T$'s are added together, three for each pump wavelength.

Also, for each pump wavelength, the algorithm may be run either: (i) without specifying the signal and idler transverse modes (in which case 15 mode combinations must be tested for each pair of peaks), or (ii) restricting to the experimentally-measured signal and idler transverse modes. Of course both alternatives should lead to the same result, which constitutes a useful self-consistency test (which is indeed fulfilled in our implementation). Our algorithm leads to a number of solutions for the fiber parameters $\{r_0, NA, \Delta, \Delta_p\}$, all of them involving the processes shown in bold typeface in Table I. In Fig. 4 we have plotted the transverse modes that participate in each of the three processes.

In addition to the determination of the specific processes present in our source, our GA yields a family of parameter sets $\{r_0, NA, \Delta, \Delta_p\}$, each one leading to agreement to within 1.5 nm between measured and predicted peaks. This parameter set family is represented with red squares in Figs. 5(a)–5(d), with the resulting values of Δk_T plotted in the vertical axis, and where black lines represent interpolations, which suggest a continuum of solutions; indeed, we verified that any combination of parameters from these curves yields good agreement with our experimental results. In Figs. 5(a) and 5(e) we have included for convenience the core radius in the bottom and the mean-field diameter (MFD) of the fundamental mode in the top. Note that while the variation along this continuum of the birefringence parameters Δ and Δ_p is only slight, there is a much more significant variation in the radius and the numerical aperture. Our family of solutions is represented in $\{r_0, NA\}$ space in Fig. 5(e), indicating what may be regarded as a continuum of equivalent fibers all of which would yield a similar SFWM behavior. Indeed, since the waveguide contribution to the overall fiber dispersion is proportional to the index contrast, i.e., to the *NA*, and inversely proportional to the core radius, the inverse relationship implied by Fig. 5(e) agrees with intuition.

Among the family of solutions shown in Fig. 5, there are two which are of particular interest. The first one, which involves the parameters $r_0 = 1.45 \mu\text{m}$ (implying a mean field diameter of $MFD = 3.27 \mu\text{m}$), $NA = 0.20$, $\Delta = 2.38 \times 10^{-4}$, and $\Delta_p = 4.57 \times 10^{-4}$ is the one that minimizes the fitness function Δk_T . The second one, which involves the parameters

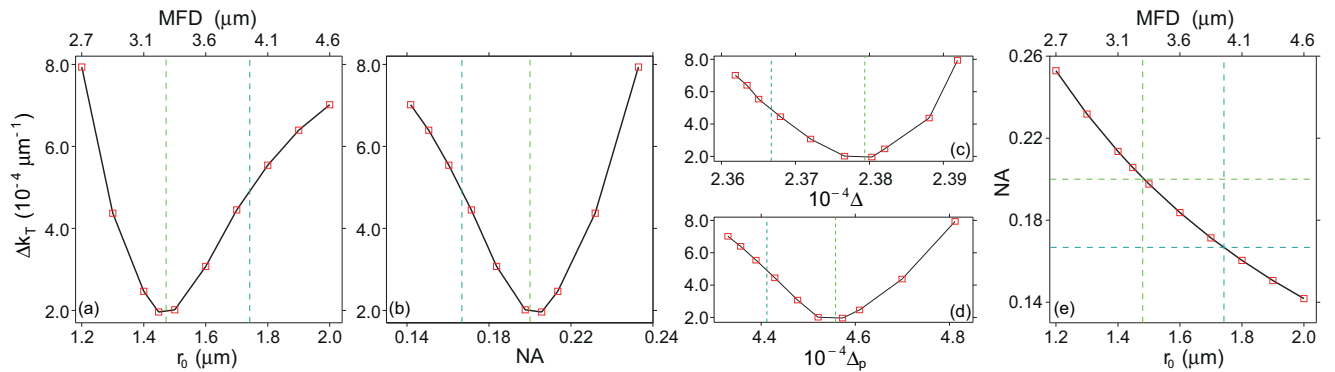


FIG. 5. For the family of solutions that we obtain, we plot the fitness function Δk_T vs core radius in (a), vs numerical aperture in (b), vs birefringence in (c), and vs parity birefringence in (d). Red dots: solutions obtained from the GA; black solid line: interpolation. In (e) we represent the family of solutions in the space formed by the core radius and the numerical aperture. Blue dotted line: data from manufacturer, green dotted line: leads to minimum fitness function.

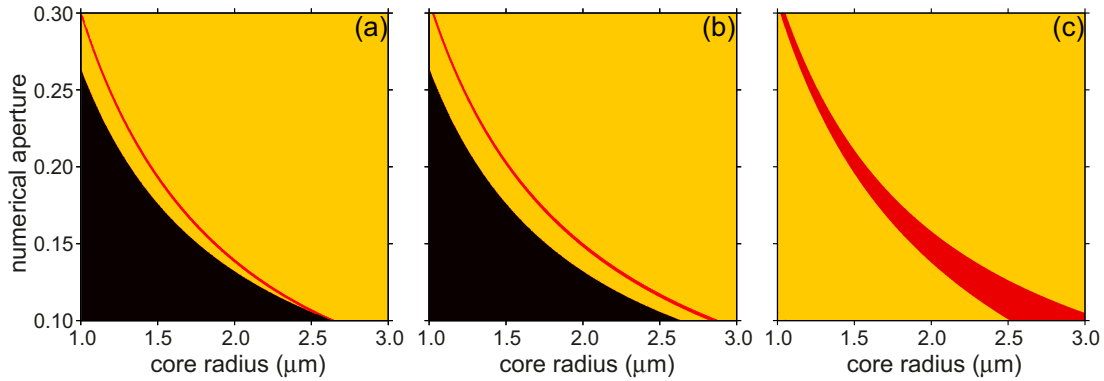


FIG. 6. Phase-mismatch function $L|\Delta k|$ for (a) process A, (b) process B, and (c) process C, plotted as a function of the core radius and numerical aperture for fixed birefringence parameters. Red regions indicate $L|\Delta k| \leq 2\pi$, yellow regions indicate $L|\Delta k| \geq 2\pi$, while black regions indicate that the non-fundamental modes LP_{11} are not supported.

$r_0 = 1.742\mu\text{m}$ (implying a mean-field diameter of $MFD = 4\mu\text{m}$), $NA = 0.167$, $\Delta = 2.37 \times 10^{-4}$, and $\Delta_p = 4.41 \times 10^{-4}$, is compatible with the parameter values provided by the manufacturer (except for the parity birefringence Δ_p , which is unspecified). The first (second) of these identified solutions involves a maximum deviation between the experimental and theory peaks of 0.59 nm (1.47 nm). In Figs. 3(c) and 3(d) we have shown phase-matching curves (i.e., defined as the locus of pump and SFWM wavelengths for which $\Delta k = 0$ for each of the three processes) overlapped with experimental points. Note the solid lines were plotted assuming the first solution from the previous paragraph, while dashed lines were plotted assuming the second solution. It is evident from this plot that: (i) the two solutions identified in the previous paragraph yield essentially the same phase-matching characteristics, and (ii) there is excellent agreement between theory and experiment.

A relevant aspect of our analysis of the experiment is that it could be exploited as a fiber characterization technique, applicable to different fiber geometries. As has been shown above, from a set of SFWM wavelength vs pump wavelength experimental data, our genetic algorithm is capable of identifying a family of parameters $\{r, NA, \Delta, \Delta_p\}$ as candidates to describe the fiber used. For the specific experimental situation studied here, on the one hand the two birefringence parameters Δ and Δ_p are relatively constant within the resulting family of solutions, and can be determined with an accuracy of $<1\%$ for Δ and $<10\%$ for Δ_p . On the other hand, the radius and numerical aperture exhibit a particular inverse relationship between them, so that the independent determination of either of these two parameters would enable us to determine the remaining parameter.

In the context of the possible application of our experimental analysis as a fiber characterization technique, it is interesting to compare the phase-matching constraints for process C (for which all waves propagate in the fundamental mode), on the one hand, and for processes A and B (which involve non-fundamental modes), on the other hand. In Fig. 6 we show, in the space formed by the core radius and the numerical aperture, the phase-matched region for which $|L\Delta k| \leq 2\pi$ for each of the three processes (red regions). Clearly, processes A and B lead to considerably more acute phase-matching constraints as compared to process C.

This implies that the existence of processes which involve higher-order modes improve the prospects of this analysis as a fiber characterization technique. Nevertheless, this fiber characterization technique could also be applied in benefit of the considerable body of work that exists based on SFWM in birefringent fibers without the use of multiple transverse modes [13–16].

V. CONCLUSIONS

We have presented a theoretical and experimental study of a photon pair source based on the process of spontaneous four-wave mixing (SFWM), in a situation where more than one transverse mode is supported, both for the pump and for the signal and idler photons. We have based our work on a birefringent fiber, specifically on a bowtie fiber, in which the propagation modes are well approximated by the linearly polarized (LP) family of modes. We discuss that in the presence of birefringence, while the fundamental mode LP_{01} unfolds into two nondegenerate modes associated with x and y polarizations, the LP_{11} (along with all those with $l \geq 1$) unfolds into four nondegenerate modes labeled by the different combinations of x/y polarizations and even or odd parity. We have shown that within the linearly polarized approximation, among all possible SFWM processes defined by different combinations of transverse modes for the four participating waves, the departure from circular symmetry means that both orbital angular momentum and parity must be conserved in order for a process to be viable. We discuss that the presence of multiple SFWM processes leads, in general, to hybrid two-photon entanglement in frequency and transverse mode.

We present the results of an experiment in which we have measured, for a number of different pump wavelengths, the SFWM spectra in coincidence, which are composed of multiple (in this case three) pairs of energy-conserving peaks. We use these experimental results, together with information about the transverse modes in which the signal and idler photons are generated, as input to a genetic algorithm, which on the one hand enables us to match a particular SFWM process with each pair of energy-conserving peaks, and on the other hand permits us to characterize the fiber, i.e., to obtain numerical values for the fiber parameters. We believe that these

results will pave the way for further progress in the generation of photon pairs in optical fibers with hybrid entanglement in frequency and transverse mode.

ACKNOWLEDGMENTS

This work was supported by CONACYT (Grants No. 230072, No. 222928, No. 253366, and No. 221052) and by PAPIIT (UNAM), Grant No. IN1050915.

-
- [1] M. Fiorentino, P. L. Voss, J. E. Sharping, and P. Kumar, *IEEE Photon. Technol. Lett.* **14**, 983 (2002).
- [2] D. C. Burnham and D. L. Weinberg, *Phys. Rev. Lett.* **25**, 84 (1970).
- [3] S. Randel, R. Ryf, A. Sierra, P. J. Winzer, A. H. Gnauck, C. A. Bolle, R.-J. Essiambre, D. W. Peckham, A. McCurdy, and R. Lingle, *Opt. Express* **19**, 16697 (2011).
- [4] Y. Chen, W. J. Wadsworth, and T. A. Birks, *Opt. Lett.* **38**, 3747 (2014).
- [5] I. Shavrin, S. Novotny, and H. Ludvigsen, *Opt. Express* **21**, 32141 (2013).
- [6] A. Christ, K. Laiho, A. Eckstein, T. Lauckner, P. J. Mosley, and C. Silberhorn, *Phys. Rev. A* **80**, 033829 (2009).
- [7] R. Kruse, F. Katzschmann, A. Christ, A. Schreiber, S. Wilhelm, K. Laiho, A. Gábris, C. S. Hamilton, I. Jex, and C. Silberhorn, *New J. Phys.* **15**, 083046 (2013).
- [8] M. Karpinski, C. Radzewicz, and K. Banaszek, *Appl. Phys. Lett.* **94**, 181105 (2009).
- [9] M. F. Saleh, B. E. A. Saleh, and M. C. Teich, *Phys. Rev. A* **79**, 053842 (2009).
- [10] P. J. Mosley, A. Christ, A. Eckstein, and C. Silberhorn, *Phys. Rev. Lett.* **103**, 233901 (2009).
- [11] L. Neves, G. Lima, A. Delgado, and C. Saavedra, *Phys. Rev. A* **80**, 042322 (2009).
- [12] D. Cruz-Delgado, J. Monroy-Ruz, A. M. Barragan, E. Ortiz-Ricardo, H. Cruz-Ramirez, R. Ramirez-Alarcon, K. Garay-Palmett, and A. B. U'Ren, *Opt. Lett.* **39**, 3583 (2014).
- [13] B. J. Smith, P. Mahou, O. Cohen, J. S. Lundeen, and I. A. Walmsley, *Opt. Express* **17**, 23589 (2009).
- [14] Q. Zhou, W. Zhang, T. Niu, S. Dong, Y. Huang, and J. Peng, *Eur. Phys. J. D* **67**, 202 (2013).
- [15] B. Fang, O. Cohen, and V. O. Lorenz, *J. Opt. Soc. Am. B* **31**, 277 (2014).
- [16] J. Fan and A. Migdall, *Opt. Express* **15**, 2915 (2007).
- [17] K. Garay-Palmett, H. McGuinness, O. Cohen, J. Lundeen, R. Rangel-Rojo, A. B. U'Ren, M. Raymer, C. McKinstrie, S. Radic, and I. A. Walmsley, *Opt. Exp.* **15**, 14870 (2007).
- [18] D. Cruz-Delgado, R. Ramirez-Alarcon, E. Ortiz-Ricardo, J. Monroy-Ruz, F. Dominguez-Serna, H. Cruz-Ramirez, K. Garay-Palmett, and A. B. U'Ren (unpublished).
- [19] A. W. Snyder and W. R. Young, *J. Opt. Soc. Am.* **68**, 297 (1978).
- [20] B. Y. Kim, J. N. Blake, S. Y. Huang, and H. J. Shaw, *Opt. Lett.* **12**, 729 (1987).
- [21] A. Mair and A. Vaziri, G. Weihs and A. Zeilinger, *Nature (London)* **412**, 313 (2001).
- [22] H. H. Arnaut and G. A. Barbosa, *Phys. Rev. Lett.* **85**, 286 (2000).
- [23] G. A. Barbosa, *Phys. Rev. A* **76**, 033821 (2007).
- [24] S. Feng and P. Kumar, *Phys. Rev. Lett.* **101**, 163602 (2008).
- [25] G. A. Barbosa, *Phys. Rev. Lett.* **103**, 149303 (2009).
- [26] S. P. Walborn, S. Padua, and C. H. Monken, *Phys. Rev. A* **71**, 053812 (2005).
- [27] D. Bharadwaj, K. Thyagarajan, M. Karpinski, and K. Banaszek, *Phys. Rev. A* **91**, 033824 (2015).
- [28] See, for example: C. Lin and M. A. Bosch, *Appl. Phys. Lett.* **38**, 479 (1981); C. Lesvigne, V. Couderc, A. Tonello, P. Leproux, A. Barthlmy, S. Lacroix, F. Druon, P. Blandin, M. Hanna, and P. Georges, *Opt. Lett.* **32**, 2173 (2007); J. Cheng, M. E. V. Petersen, K. Charan, K. Wang, C. Xu, L. Gruner-Nielsen, and D. Jakobsen, *Appl. Phys. Lett.* **101**, 161106 (2012).
- [29] F. Poletti and P. Horak, *J. Opt. Soc. Am. B* **25**, 1645 (2008).
- [30] Y. Ding, J. Xu, H. Ou, and C. Peucheret, *Opt. Express* **22**, 127 (2014).
- [31] E. Meyer-Scott, V. Roy, J-P. Bourgoin, B. L. Higgins, L. K. Shalm, and T. Jennewein, *Opt. Express* **21**, 6205 (2013).
- [32] Q. Lin, F. Yaman, and G. P. Agrawal, *Phys. Rev. A* **75**, 023803 (2007).
- [33] J. Noda, K. Okamoto, and Y. Sasaki, *J. Lightwave Technol.* **4**, 1071 (1986).
- [34] Z. Wang, J. Ju, and W. Jin, *Opt. Express* **13**, 4350 (2005).
- [35] Note that while the cutoff wavelength for the LP₁₁ mode is 759 nm, our approximate dispersion model cannot predict the cutoff wavelengths for the LP₁₁^{ex} and LP₁₁^{ox} modes.